Stochastic modelling suggests that an elevated superoxide anion - hydrogen peroxide ratio can drive extravascular phagocyte transmigration by lamellipodium formation

Siddhartha Kundu [a,b,c,][*][,1]

[a] Department of Biochemistry, Dr. Baba Saheb Ambedkar Medical College & Hospital, Government of NCT Delhi, Sector – 6, Rohini, Delhi 110085, India
[b] Mathematical and Computational Biology, Information Technology Research Academy (ITRA), Media Lab Asia, 2nd Floor, Block 2, C-DOT Campus, Mehrauli, New Delhi 110030, India
[c] School of Computational and Integrative Sciences, Jawaharlal Nehru University, New Mehrauli Road, New Delhi 110067, India

H I G H L I G H T S

- Aggregates of higher order RRA-oligomers may facilitate lamellipodium formation.
- RRA-oligomer driven free radical accumulation can prolong membrane perturbation.
- The response curve of ECSOD is bimodal, and is separated by a steady-state phase.
- There is an inverse association between superoxide anions and hydrogen peroxide.

A R T I C L E   I N F O

A B S T R A C T

Chemotaxis, integrates diverse intra- and inter-cellular molecular processes into a purposeful pathophysiological response; the operatic rules of which, remain speculative. Here, I surmise, that superoxide anion induced directional motility, in a responding cell, results from a quasi pathway between the stimulus, surrounding interstitium, and its biochemical repertoire. The epochal event in the mounting of an inflammatory response, is the extravascular transmigration of a phagocyte competent cell towards the site of injury, secondary to the development of a lamellipodium. This stochastic-to-markovian process conversion, is initiated by the cytosolic-ROS of the damaged cell, but is maintained by the inverse association of a *de novo* generated pool of self-sustaining superoxide anions and sub-critical hydrogen peroxide levels. Whilst, the exponential rise of $O_2^{.-}$ is secondary to the focal accumulation of higher order lipid raft-Rac1/2-actin oligomers; $O_2^{.-}$ mediated inactivation and redistribution of ECSOD, accounts for the minimal concentration of H_2O_2 that the phagocyte experiences. The net result of this reciprocal association between ROS/ RNS members, is the prolonged perturbation and remodeling of the cytoskeleton and plasma membrane, a prelude to chemotactic migration. The manuscript also describes the significance of stochastic modeling, in the testing of plausible molecular hypotheses of observable phenomena in complex biological systems.

© 2016 Elsevier Ltd. All rights reserved.

1. Introduction

The chemically driven motion of a cell (chemotaxis), is the migration of cells along a concentration gradient of a particular chemical moiety. This conserved evolutionary phenomenon is commonly seen in endothelia, neutrophils and monocyte-macrophages of higher organisms, as well as, in simple eukaryotes (*Dictyostelium discoideum*) and prokaryotes. The chemical structure notwithstanding, inductive behavior in a cell, for a particular compound, depends on a dynamic clustering of a multitude of factors. The proposed mechanisms involve flagellar clockwise
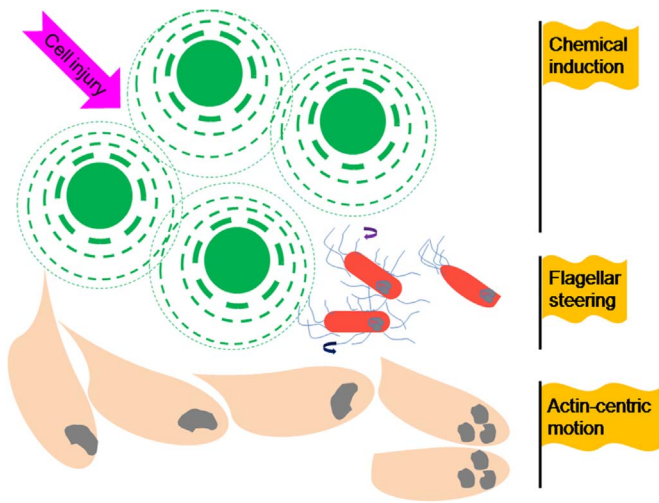
Fig. 1. Chemotactic motility in diverse organisms. The movement of cells towards a chemical moiety is as diverse as the organisms themselves and includes: flagellar rotation, pseudopodia generation, and amoeboid motion. Both, attractant and repellant mobility have been demonstrated under laboratory conditions. The inflammatory response in tissues is spatio-temporal with the release of damaging free radicals or their precursors secondary to cellular injury, increased vascular permeability, diapedesis, and transmigration of phagocytic competent cells towards a chemo-attractant(s).

(CW) and counter-clockwise (CCW) motions, coordinated microspike and bleb development (*D. discoideum*), and F-actin mediated pseudopodia generation (Fig. 1) (Yousif et al., 2015; Lin et al., 2015; Tyson et al., 2014; Brown et al., 2002). The resultant movement may either be convergent (chemoattractant) or divergent (chemorepellant). In *Escherichia coli*, the chemical nature of the inducer determines the quanta of movement. Attractants include: serine, aspartic acid, and glucose, while repellants such as fatty acids constitute the noxious component of the stimulus (Edgington and Tindall, 2015; Nagy et al., 2015; Pasupuleti et al., 2014; Danielson et al., 1994). These effects are mediated by extensive signal transduction networks, downstream of at least five transmembrane receptors (Shimaoka et al., 2004; Borkovich et al., 1989). In higher organisms, the progesterone secreted by the cumulus oophorous influences spermatozoal movement when in proximity with the ovum (Guidobaldi et al., 2008). The social amoeba, *D. discoideum*, exhibits a trimodal life cycle. The transition from the stage of nutritional deprivation to one of surplus, results in a shift from unicellular morphology to an elaborate multicellular sessile fruiting body. This is facilitated by an intermediate aggregate form referred to as the 'slug'. Chemotaxis, is exhibited early in the lifecycle with the stimuli being folic acid (FA) and cyclic-adenosine monophosphate (cAMP) (Wessels et al., 2014; Srinivasan et al., 2013; Segota et al., 2013).

Inflammation, an innate immune reaction to noxious stimuli (infection, injury), is initiated when the first line of host defense is breached, *i.e.*, a compromise in the integrity of anatomical- (skin and acidic pH of the gastric mucosa) and physiological-barriers. This generic patho-physiological response is characterized by: local hyperemia and raised skin temperature (secondary to chemical vasodilation), swelling (exudation of fluid into the interstitial space through endothelial gap widening), pain (involvement of nerve endings), and tissue damage (phagocytosis following diapediasis, extravasation, and transmigration). The inflammatory process, within tissues, maybe secondary to a range of causal irritants, *viz.*, physical, infective, chemical. These covert occurrences, however, are not entirely benign and are often precursors to a long term systemic pathology (dysplasia and squamous cell carcinoma; atherosclerosis and cardiovascular disease; inflammatory bowel disease; hepato-biliary pathology as in steatosis, hepatitis, cirrhosis, and hepatocarcinoma). Mediators of inflammation could be chemokines, free radicals, an acid/base environment, among several others. Reactive oxygen species (ROS), are a molecular ensemble of free radicals and metabolic intermediates and comprise superoxide anions ($O_2^{\cdot-}$), hydrogen peroxide (H_2O_2), hydroxyl radicals ($\cdot OH$) and hydroxide ions (OH^-). These occur in tandem with the reactive nitrogen species (RNS) of $ONOO^-$, NO^-, and NO_2. ROS, as signaling molecules regulate the balance between cellular proliferation and senescence, influence the magnitude of immune response, and participate in cytoskeleton remodeling and migration (Forman et al., 2004; Torres and Forman, 2003; Mikkelsen and Wardman, 2003). The concentration of free radicals in biological systems is dependent on the interleaved processes of initiation, propagation, and termination. The principal sources of ROS are enzymes either as a primary product (Xanthine oxidase, EC 1.17.3.2; NADP(H) oxidase, EC 1.6.3.1; Nitric oxide synthase, EC 1.14.13.39) or secondary to diffusion from the active site (2-oxoglutarate dependent dioxygenases, EC1.14.11.x) (Kundu, 2015a, 2015b; Rocklin et al., 2004). The pathways that contribute to maintaining this chain reaction result in the generation of substrate radicals, and include the hydro- and endo-peroxides of unsaturated membrane lipids (Lipoxygenases, EC 1.13.11.x) or hypohalous acid (Myeloperoxidase, EC 1.11.2.2). Terminators of this cascade include dismutation, either enzymatic (Superoxide dismutase, EC 1.15.1.1; Catalase, EC 1.11.1.6; Glutathione peroxidase, EC 1.11.1.9) or spontaneous self-association; small molecule scavenging (ascorbic acid, urea, retinol, tocopherols), and intracellular transport by the chloride anion transporter-3 (ClC3) (Fisher, 2009; Hawkins et al., 2007).

In the absence of an overt ciliary or flagellar contributory influence, the cytoskeletal network in cells remains a watershed of subtle chemical fluctuations that transpire extracellularly. Migration may be in response to a gradient of morphogens (embryonic tissue patterning), or to mitigate the effects of a noxious stimulus (neutrophils, monocyte-macrophages). The signal transduction route usually involves GTP-binding protein(s), secondary messengers, and several cycles of kinase-phosphatase activity (Sadhu et al., 2003; Sakai et al., 2003; Sastry et al., 2002; Zervas et al., 2001; Angers-Loustau et al., 1999; Tamura et al., 1998; Allen et al., 1997; Nobes and Hall, 1995; Chen and Guan, 1994). Monomeric GTPase (Rac, Rho, and Cdc42) driven motility is accomplished by extending lamellipodia at a leading edge, with a concomitant retraction of the lagging end (Wong et al., 2006; Van Keymeulen et al., 2006; Tzima, 2006; Watanabe et al., 2004; Fukata et al., 2003; Allen et al., 1997). Since the formation of membrane bound cytoplasmic extensions is, inherently stochastic, with several extrusions developing in parallel, the final outcome may be a function of a molecular filter that may function to sense and modulate the chemically defined signaling gradient (Kundu and Subodh, 2011; Hattori et al., 2010; Andrew and Insall, 2007). The output of this hypothetical unit could then initiate the appropriate feedback mechanism(s) by actuating downstream pathways, thereby, ensuring the maturation of a single dominant extension with consequent vectorial movement. A role, *albeit*, indirect, for ROS/RNS in this cell steering activity has been postulated and investigated (Kundu and Subodh, 2011; Hattori et al., 2010; Andrew and Insall, 2007). The emphasis of much of this work was on the hydrogen peroxide mediated activation of the GTPase-PLC/D-calcium/PTEN or Axl-PI3K-Akt1 transduction axes to bring about migration secondary to redox-based cytoskeletal rearrangement (Huang et al., 2013; Andrew and Insall, 2007; Fischer et al., 2005; Usatyuk et al., 2003; Vepa et al., 1999; Hastie et al., 1998; Natarajan et al., 1996). However, H_2O_2 is a potent phosphatase inhibitor, and can rapidly increase the pool of kinase-mediated phophorylated proteins. This phosphate-sink, can deplete the cell of available ATP, saturate the

transduction pathways, result in cell cycle arrest and senescence, and inhibit migration due overpolymerization of F-actin (Shi et al., 2014; Kim et al., 2012; Guyton et al., 1996; Kawakami et al., 1996; Volberg et al., 1991). This apparent contradiction depends on the dose of H_2O_2 that the cell experiences. Whilst, low concentrations enhance migration and proliferation, high levels result in irreversible senescence (Kim et al., 2012; Zhou et al., 2011; Park et al., 2006).

The major premise explored in this work is that the responding cell is able to maintain sub-critical levels of H_2O_2, while generating and maintain exponential concentrations of membrane derived extracellular phagocyte O_2^-. Clearly, for these short-lived intermediates to function as signal transducers, their half-lives $(t_{1/2})$ must be extended. Here, I explore two facets, *i.e.*, self-sustained generation and terminator exhaustion, either exclusively, or intandem, as causal, for these changes. The plasma membrane bound and stimuli dependent leukocyte NAD(P)H-oxidase is assembled in real time secondary to successful twin translocations of the $p40^{phox}$–$pp47^{phox}$–$p67^{phox}$ complex and the Rho-GTPase (Rac1/2) to the membrane, in tandem with the turnover of secretory vesicle and granule bound $p22^{phox}$–$gp91^{phox}$ complex (Babior, 1999). Additional, critical components of this stimulus driven real time network are ECSOD, lipid rafts (ordered microdomains of 8–200 nM enriched in cholesterol, sphinomyelin, and saturated fatty acyl chains), and F-actin. The postulated response curve is, therefore, likely to be flat with a slow sustained rise followed by multiplet peak(s); a pattern suggestive of repeat cycles of superoxide production by the phagocytosis-competent cell. This continuum of cytoskeletal associated membrane remodeling is critical to the development of direction-specific lamellipodium formation. Mathematical modeling, despite its speculative nature offers investigators insights into phenomena that are observed with difficulty, or, not at all. Most models equate the change in the quantity of a dependent- with one or more independent-variable(s). The solution to these ordinary-, partial-, or stochastic-differential equations (ODEs, PDEs, SDEs) may be ascertained analytically or numerically. Deterministic methods (ODEs, PDEs) are specific for a particular set of conditions and are iteration invariant. SDEs, usually entail the formulation of a chemical master equation (CME), and permit an unbiased evolution of the modeled metabolites (Wylie et al., 2007; Nicolau et al., 2006). This work focuses on modeling the origins of a dominant pseudopodium, a critical early stage event in the response of an immune-competent cell to a necrotizing stimulus. Additionally, plausible scenarios linking the molecular components of this real-time network with macro-observable phenomena are presented and analyzed.

2. Results

2.1. Putative plasma membrane dynamics

In an uninduced/unbiased cell the component molecules: (a) exhibit similar Michaelis Menten constants, $\left(\text{non} - \text{enzymatic}; k_a \stackrel{\text{def}}{=} k_m = k_{-1}/k_1\right)$, and (b) switch rapidly between the bound and unbound states. This scenario, clearly leads to the occurrence of a steady-state equilibrium wherein, membrane blebs/spikes/protrusions, despite their frequency remain transitory and non-collegial. The probability scores of individual nodes for this model (SSM1) were computed as under and combined Eqs. (1) and (12).

$$P_{ij} = \begin{cases} P_{kj} + \phi_i, & j^{th} \text{ node of } k^{th} \text{ observation corresponding to } \phi_i \\ |P_{kj} - \phi_i|, & j^{th} \text{ node of } k^{th} \text{ observaton with value that exceeds } \phi_i \end{cases} \quad (1)$$

Here, the quantity $\left(\phi_i = \min\left(a_{ij}/\sum a_{ij}\right)\right)$, is used to determine the
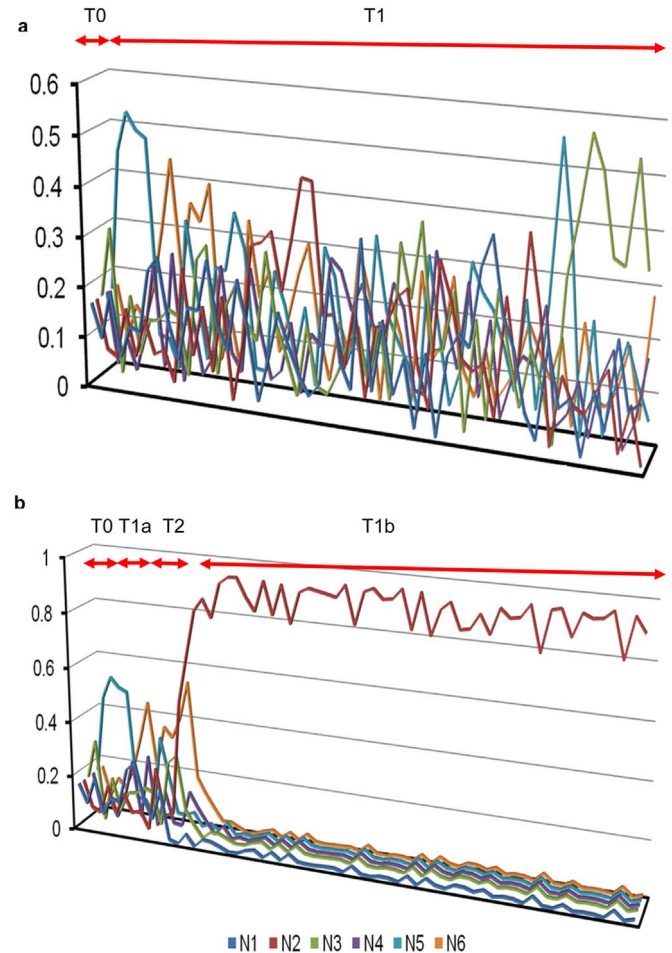

Fig. 2. Static stochastic models of the membrane dynamics of a phagocyte in the presence of a chemoattractant. (A) Here, despite the proximity of the inducer, membrane activity is random and self-limiting. The response is characteristically bi-phasic with an equal probability of all membrane loci developing a dominant extrusion (T0), and inconsequential fluctuations that persist indefinitely (T1) until the inducer is removed, (B) in this representation, the response of the approaching cell may comprise three phases. While, T0 and T1a are as above, T2, suggests additional involvement of one or more molecular switches and signal accumulators. Stochasticity resumes at the reset baseline (T1b).

probability of forming a dominant lamellipodium, from a cluster of nodes present at a finite distance from the stimulus $\left(P_{ij}^{final}\right)$. Since, $0 < \phi \le b < 1; k = i - 1$, it follows that $0 < P_{ij} \lesssim P_{kj} < 1$; $\lim_{P_{ij} \to 1} P_{ij}^{final} \to 0$ (Fig. 2A; Table S1A; Dataset S1). On the other hand, the introduction of a defined chemical attractant results in the actuation of several downstream events, of which, most notably, is the local restructuring of the plasma membrane in association with elements of the cytoskeleton. This induced bias is modeled and combined Eqs. (2) and (12).

$$P_{ij} = \left(P_{kj}\right)\left(\phi_i\right) \quad (2)$$

Similarly, for the same numerical values, it follows that $P_{ij} < P_{kj}$; $\lim_{P_{ij} \to 0} P_{ij}^{final} \to 1$. This implies that the dominant extrusion can be formed and maintained indefinitely (Phase T1b) $\left(mean \cong 0.93, sd \cong 0.06, N_{obs} = 49\right)$ (Fig. 2B, Table S1B, Dataset S2).

2.2. Computation of a threshold for the O_2^- binary response

Oligomers of lipid rafts, NADP(H) oxidase, and F-actin, and the generated superoxide anions (Table 1, Tables S2 and S3), were

utilized as components of a suitably formulated chemical master equation. The model parameters were adjusted empirically so as to correspond with RRA-complex formation of ratios greater than a predefined lower bound (Ψ_{12}; Ψ_{24}; $\Psi_{48} \geq 2.00$). The rationale for this was that the imposition of a theoretical lower bound in an otherwise stochastic setting would ensure that the molecular products, *viz.*, di-, tetra-, and octa-meric forms of the RRA-complexes were at most 50% of the reactants, *i.e.*, mono-, di-, and tetra-mer forms. Whilst, the data for the lower order oligomers (Ψ_{12}, Ψ_{24})

was readily available, the same for Ψ_{48} needed interpolation. These, when taken in context of the aforementioned ratios, in particular the consistently higher ($\Psi_{48} \geq 3.00$), implies an inhibitory effect of high concentrations of ECSOD on RRA_{8+} formation (Table S4A), and suggests that higher-order oligomerization could be a critical factor in the genesis of pseudopodia with vectorial bias.

Threshold selection for the static models (SSM -1, -2) was based on the results of the *in silico* simulations carried out, *vide infra*. Data from the DSMs suggest that the ratio $RRA_4/RRA_8(\Psi_{48})$ (Table S4A),

Table 1
Summary of mathematical models utilized in this work.

S. no	Mathematical models		Features	Remarks
1.	Static stochastic	SSM1	$N_{obs}=53$	• Baseline membrane fluctuations (Eqs. (1) and (12))
				• Biphasic (T0, T1)
		SSM2	$N_{obs}=62$	• Switch mechanism for lamellipodium formation (Eqs. (2) and (12))
				• Threshold dependent
				• Triphasic (T0, T1, T2)
2.	Dynamic stochastic	DSM (1–4)	$N_{obs}=90$	• Median of timesteps of each experiment
			$N_{exp}=3$	• Incorporation into linear model (Eq. (13))
			$N_R=15$	• Analysis of interpolated data in triplicate
			$N_{Rn}=26$	
3.	Regression	DSM (1–4)	$N_{obs}=100$	• ECSOD-RRA/RRA$_+$ (Eqs. (3)–(5))
			$N_{obs}=1000$	• ECSOD-RRA$_n$ (Eqs. (6)–(9))
				• Equilibrium analysis (Eqs. (15) and (16))
				• Threshold determination (Eq. (14))

Abbreviations
N_{obs}: Number of observations
N_{exp}: Number of distinct experiments
N_R: Number of reactants
N_{Rn}: Number of biochemical reactions.

Fig. 3. Non-linear regression analysis. Scatter plots of ECSOD and RRA-complexes were constructed from interpolated data using the dynamic stochastic models (DSMs 1–4) as the source. The curves of equations relating levels of ECSOD (coordinate axis) with RRA-complexes (ordinate axis) (Eqs. (6–9)) were plotted (A–D). Since, the focus of this analysis was the selection of a curve that differed significantly from the baseline, the curve (D) representing Eq. (9) was shortlisted for further interpretation.

would be most appropriate, *i.e.*, exhibit maximal variance $\left(\sigma_{12}^2 \cong 0.0011, \sigma_{24}^2 \cong 0.0015, \sigma_{48}^2 \cong 0.1923; \text{Eqs. (3)–(5)} \right)$. Analysis of the regression equations $(y := \Psi_{48})$ for the datapoints $(0 < x := ECSOD \le 50000; N_{obs} = 100)$ suggest that variance of the data may be a better index, as compared to the coefficient of determination (R^2), in making this selection $(\sigma_{poly}^2 \cong 8764.259, \sigma_{ln}^2 \cong 0.04716, \sigma_{power}^2 \cong 0.053084)$ (Table S4B). Further, since the main objective was to identify the ratio $\left(\Psi_{48} \middle| \Psi_{48} \ge 2.00 \right) \wedge \left(min \middle| \Psi_{48,obs} - \Psi_{48,computed} \middle| \right)$, the natural log function of ECSOD (Eq. (4)) was chosen as it was the closest approximation to the modeled data $\left(\sigma_{min}^2, slope_{min} \right)$. This corresponded to $\lceil ECSOD \rceil \cong 5E-06 \, aM$ and $\Psi_{48} \cong 2.922091$, which was incorporated into Eq. (14) and used to compute the threshold value $(\omega \cong 0.465 \cong 0.50)$ (Tables S1B and S4C).

$$y_{poly} = 3E-13x3 - 2E-08x2 + 0.000x + 2.691; R^2 = 1 \qquad (3)$$

$$y_{ln} = (0.234)\ln(x) + 1.475; R^2 = 0.861 \qquad (4)$$

$$y_{power} = (1.908)x^{0.069}; R^2 = 0.846 \qquad (5)$$

2.3. Superoxide anion levels

The hypothesis explored here, is that localized ROS/RNS can push the cellular machinery over a dynamically-defined threshold, and thereby, drive the formation of a dominant extrusion. Statistical analysis of the non-linear regression curves of the results of the RRA-complexes with functionally available ECSOD (Eqs. (6)–(9); Fig. 3, Tables S3, S5 and S6) does not suggest any clear preference $\left(t_{12}^{stat} \cong 68.16, t_{14}^{stat} \cong 26.91, t_{18}^{stat} \cong 37.22; P(t \le T) \le 1.0E-47; t_{crit}^{one-tail} \cong 1.66, t_{crit}^{two-tail} \cong 1.98; df = 100 \right)$. However, the ratios of the variance data, *i.e.*, F-statistic for these datapoints $(F_{12}^{stat} \cong 2.22, F_{14}^{stat} \cong 1.97, F_{18}^{stat} \cong 1.40; F_{crit} \cong 1.39; df = 100)$, suggests that Eq. (9) is a superior approximator of the ECSOD-RRA-RRA$_8$ data (Table S6). Validation of this assumption was sought by computing Pearson's correlation coefficient $(r_{pearson})$. Once again data modeled by Eq. (9) for the ECSOD-RRA-RRA$_8$ data performed better $(r_{pearson} \cong 0.9165)$. In contrast, data for ECSOD-RRA-RRA$_2$, ECSOD-RRA-RRA$_4$ were negatively correlated $(r_{pearson} \cong -0.90)$ (Tables S5 and S6). The regression equations may be formulated $(y = \mathcal{P}(x); degree = 3; R^2 = 1)$ as under:

$$y_1 = 1E-10x3 - 2E-05x2 + 0.516x + 11642 \qquad (6)$$

$$y_2 = 5E-10x3 - 3E-05x2 + 0.531x + 56414 \qquad (7)$$

$$y_4 = 5E-10x3 - 3E-05x2 + 0.547x + 26651 \qquad (8)$$

$$y_8 = -5E-10x3 + 3E-05x2 - 0.595x + 9732 \qquad (9)$$

y := concentration of RRA_8

x := concentration of $ECSOD$

A comparison of the absolute values of the slope $(\eta := |\Delta y / \Delta x|)$ of these curves (ECSOD vs O_2^-; Fig. 4A, Table S5B), further highlights this change $(\eta_1 \cong 0.258, \eta_2 \cong 0.319, \eta_4 \cong 0.703, \eta_8 \cong 1.800)$. The platykurtic curve of the monomer $(\kappa_1 \cong -0.237)$, contrasts with the leptokurtic versions of the oligomeric data $(\kappa_2 \cong 2.609, \kappa_4 \cong 2.308, \kappa_8 \cong 1.537)$ (Table S6). A closer examination of the curve for octamer-generated superoxide anions, reveals a plateau $(min(\eta_8) \cong 0.084; y \cong 0.080 aM)$ at the ECSOD concentrations $(0.025 - 0.043 aM)$ (Fig. 5A, Table S7), that could function as signal accumulator, thereby staggering or buffering any sudden change. The above curve-structure and data, clearly
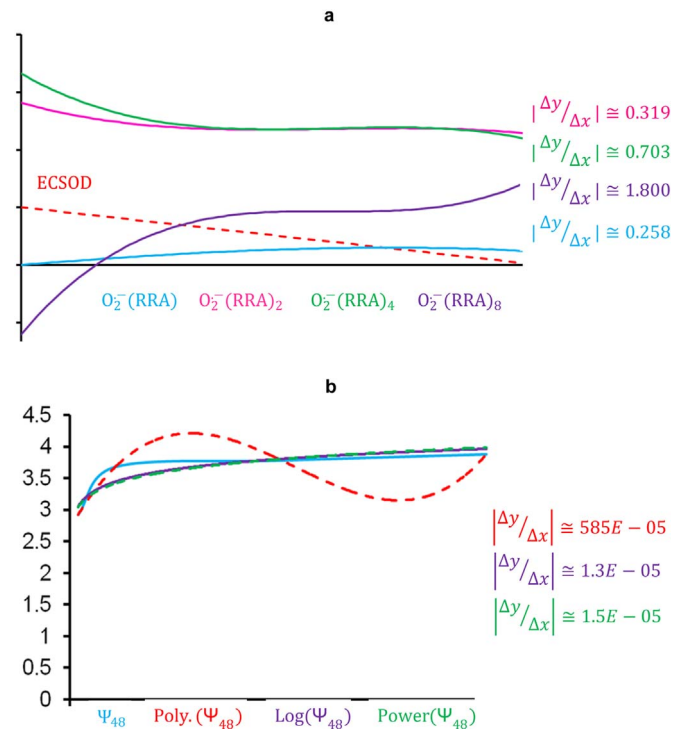

Fig. 4. Slope analysis of non linear regression curves. (A) The combined plot of curves (Eqs. (6)–(9)) were analyzed and their slope $(\Delta y/\Delta x = abs(y_{final} - y_{initial})/abs(x_{final} - x_{initial}))$ computed. The largest value (Eq. (9)) was calculated for RRA_{8+}. This implied maximal divergence for higher order RRA-complexes. (B) Data for threshold analysis was obtained and similarly analyzed. However, the selection here was more stringent since the objective was to find the [ECSOD] that corresponded to the simulation values (DSM1-4). The curve that corresponded to Eq. (4) was chosen for further analysis, $min(\sigma^2)$, $min(\Delta y/\Delta x)$.

suggests an operatic 'switch' mechanism that is surmountable, threshold-dependent, and principally mediated by high-order RRA-complexes.

3. Discussion

Molecular processes are inherently stochastic with the probability of a dominant event developing being minimal in unperturbed systems. Empirically determined data, however, suggests that this lack of bias can be easily circumvented *in vivo*, a phenomenon that highlights the inherent complexity of cell physiology.

3.1. Molecular and cellular equivalence of stochasticity

Complex systems need to be simultaneously, robust (reduced sensitivity) and ill-conditioned (highly sensitive). Whilst, the latter are auto-regulatory, self-limiting, and can serve as temporal regulators (pace makers); refractoriness of the former is desirable to introduce 'a delay'. A likely scenario in organized cells, is the existence of one or more plateau(s) in combination with spiking activity (Fig. 5A). Such a cell could then exhibit binary behavior, switching between sub- and supra-threshold states at a rate corresponding to the magnitude of this quasi-steady state. Interpreting this in molecular terms converges on a reaction mechanism(s) operating at the instance of an actuator with amplification/dampening superimposed on the baseline stochasticity; conditions reminiscent of free radical generation and scavenging (Kundu, 2015b) (Fig. 5B).

The numerical solution(s) of an appropriately formulated chemical master equation, simulated here by the DSMs, can serve to populate the coefficient matrix of an equation based on the
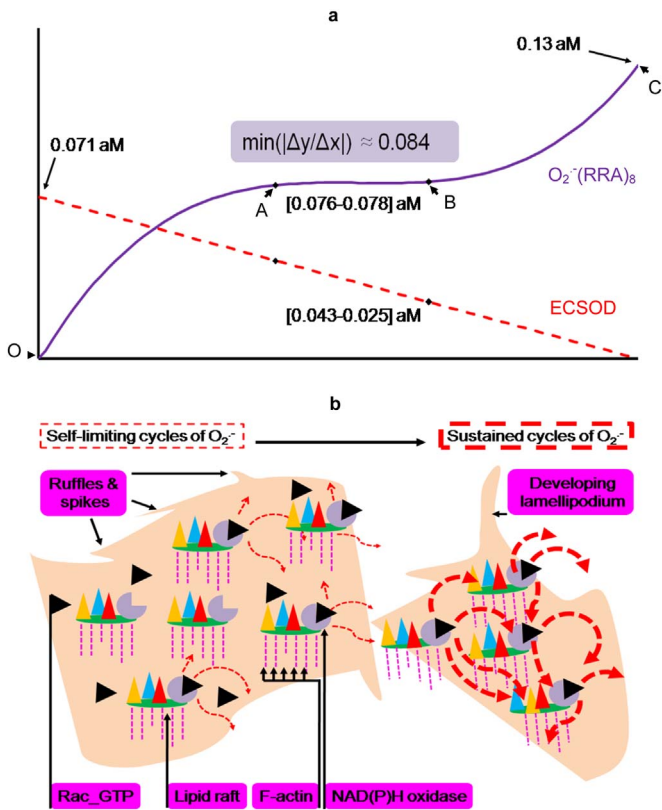
Fig. 5. Fate of superoxide anions in the genesis of a dominant lamellipodium. (A) Definition and delineation of a zone of equivalence, a critical factor in the establishment of a quasi-binary switch. This was done using equilibrium analysis of the selected curve (Eq. (9)), as outlined in Eqs. (15) and (16). (B) Schematic diagram of a biphasic rise in concentration of O_2^- in the vicinity of a responding immune-competent cell. Here, the conversion of the transient futile cycle of superoxide anion generation by lower order RRA-complex formation is dependent on the accumulation of higher order forms.

biochemical parameters of molecular half-life and kinetics (enzyme: MM, co-operative; binding) of the simulated components. The central tenet of this representation is the dependence of the chemotactic-facilitating lamellipodium $\left(P_{ij}^{final}\right)$ on the net accumulation of superoxide anions (τ).

$$P_{ij}^{final} \quad \propto \quad \tau$$
$$P_{ij}^{final} \quad = \quad (\mu)(\tau)$$
$$\mu \qquad := \quad \delta\tau/\delta T = (\tau_{formation}^0 + \tau_{formation}^1) - \tau_{breakdown}$$
$$\tau_{formation}^0 \quad := \quad \text{preformed } ROS/RNS$$
$$\tau_{formation}^1 \quad := \quad \text{denovo } ROS/RNS$$
$$\tau_{breakdown} \quad := \quad \text{dismutation} \qquad\qquad\qquad (10)$$

In this assumption, there is a dual spike $\left(\tau_{formation}^0 + \tau_{formation}^1\right)$ in the levels of free radicals (ROS+RNS). During the initial phase of a necrotizing injury to the cell, there is a deluge of these preformed $(\tau_{formation}^0)$ reactive intermediates from the cytosol of the injured cell into the extracellular matrix. The limited ECSOD levels are saturated with these. The subsequent increase in ROS $\left(\tau_{formation}^1\right)$ takes place *ab initio*. Since, the half-life of ECSOD is protracted $(\cong 85h)$, there is a substantial lag in ECSOD-mediated scavenging (Karlsson et al., 1994; Marklund 1982). The ECSOD activity and levels are further restricted by the observation that free radicals can impair its association with the extracellular matrix, as well as, downregulate transcription (Gao et al., 2008; Stralin and
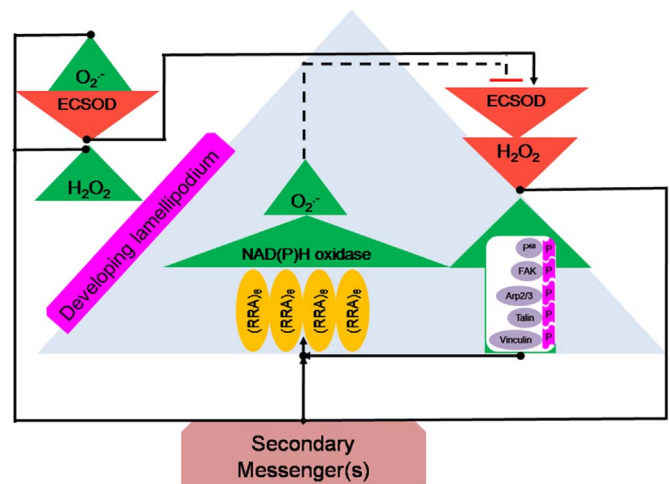

Fig. 6. Molecular mechanisms of lamellipodium formation in circulating phagocytes. An integrated model highlighting the significance of the extracellular matrix (ECSOD), intracellular transport, secondary messengers, plasma membrane components, and the cytoskeleton; in a complex interplay that results in the development of a single protrusion, thereby, steering the cell towards the stimulus. The final outcome is a self-sustaining free radical chain reaction that is responsible for the directional migration of the responding cell.

Marklund, 1994). These, when present concurrently could ensure that role of ECSOD is functionally null $(\tau_{breakdown} \to 0)$ (Fig. 6).

3.2. Higher order oligomers can mediate the exponential rise of superoxide anions

Data from these simulations suggest that O_2^- from the low order RRA-complexes result in the observed response plateau, *i.e.*, a quasi-steady state or dynamic equilibrium. However, as the association proceeds, there is a distinct spike in the levels of O_2^-. Thus, it would seem that the assembly of higher order oligomers $\left(RRA_{8+}\right)$ of the raft-ROS-actin complex is vital to this process. Any model to comprehend this observation at the molecular level, would therefore, have to link the preformed ROS, either exclusively, or in tandem with critical levels of ECSOD $\left(\tau_{formation}^0 - \tau_{breakdown} > 0\right)$. Contributory factors could include (i) the import mechanisms deployed, such as the transporter- or caveolin-based internalization of physico-chemical modifiers (Decleva et al., 2013; Ushio-Fukai, 2009; del Pozo et al., 2004), (ii) cell–cell and cell–matrix connectivity, with the cytoskeleton, plasma membrane, intgerin-protein complexes, focal adhesions, and the ECM as major proponents (Luo et al., 2007; Sakai et al., 2003; Zervas et al., 2001; Chen and Guan, 1994), and (iii) expression patterns molded by the formation of complex gene regulatory networks, secondary to secondary messengers such as PI3K, phospholipases C and D, and calcium; overlapping signal transduction pathways (p38^{MAPK}, ERK, Akt, p53-p21), nuclear translocation, and altered transcription (Huang et al., 2013; Liu et al., 2007; Hastie et al., 1998; Derevianko et al., 1997; Guyton et al., 1996; Bianchini et al., 1993).

1. A redox-based restructuring of actin and microtubular cytoskeletal elements could have important consequences for cell motility, extravasation, metastasis, trans-differentiation, and intercellular communication (cell-cell, cell-matrix) (Grigoriev et al., 2006; Nimnual et al., 2003; Moldovan et al., 1999). Mechanistic details of actin-centric movement involve the integration of numerous dynamic signaling platforms that function to transduce extracellular signals into appropriate migratory cues. The membrane 'ruffles', discussed earlier, may be correlated to the futile cycles of superoxide anion generation

below a threshold limit by lower order RRA-complexes (Fig. 5B and/or foci for the accumulating RRA_{8+}). The mechanism for this is speculative, but, could occur secondary to import of surplus O_2^- or H_2O_2, from the previous spike via the chloride anion symport or aquaporin channel into subcellular compartments wherein, the post-translational modifications of nitrosation, S-glutathionylation, carbonylation, and disulfide bridge formation of actin may be initiated (Decleva et al., 2013; Hawkins et al., 2007; Giustarini et al., 2005; Banan et al., 2000). The cross-linking of actin microfilaments (Arp2/3, cortactin) (Weed and Parsons, 2001; Weed et al., 2000; DalleDonne et al., 1995), could result in the association of plasma membrane RRA-complexes. Clearly, this route to higher-order oligomer formation would be dependent on the post-injury cellular ROS load. If, $\tau_{formation}^0 \gg \tau_{breakdown}$, then this would translate into a larger volume of vesicular transport en-route to the phagolysosome, with subsequent RRA_{8+} formation. The recursive cycles of sub-threshold plasma membrane superoxide anions and its associated spikes, could in fact be a sensing mechanism for the PML, a critical event in the conversion of a gradient signal into directed chemotaxis involving a dominant lamelipodium (Kundu and Subodh., 2011; Hattori et al., 2010; Oshikawa et al., 2010; Andrew and Insall, 2007).

2. However, the results (Fig. 5A), also suggest that the levels of available ECSOD could be important in determining the migratory potential of the PML, both, biochemically and as a scaffold protein. At least two isoforms of superoxide dismutase *sod2* and *sod3*, have been shown to influence this facet of neutrophil activity. Whilst, the effect is dose independent for *sod2*, ECSOD (*sod3*) promotes growth, proliferation, and migration at low doses, and arrest, senescence, and apoptosis at higher expression levels (Miar et al., 2015; Liu et al., 2015; Laukkanen et al., 2015; Cammarota et al., 2015; Zhang et al., 2014; Castellone et al., 2014). These findings ascribe a role for ECSOD in effecting the dynamics of well characterized pro- and anti-migratory molecules, thereby, influencing the adhesion potential of the plasma membrane, mRNA levels of transcription factors (*sod2;* C-myc*;* C-jun*;* STAT3; JNK), and the activation of small molecule GTPases (*sod3*) (Liu et al., 2015; Laukkanen et al., 2015; Cammarota et al., 2015; Jin et al., 2014; Zhang et al. 2014; Castellone et al., 2014; Luo et al., 2007; Tai et al., 2003; Sakai et al., 2003; Zervas et al., 2001; Chen and Guan, 1994). In addition, an indirect anti-inflammatory role, based on its physical association with the ECM components (heparan sulfate, hyalurnon, elastin) and plasma membrane, through the heparan-binding domain (HBD; R210-A222) has been ascribed (Olsen et al., 2004; Folz et al., 1994). This data when coupled with the results from this study hint at the cytosolic activation of Rac1/2 by vesicular ECSOD en-route to the cell membrane. Subsequent secretion and association with extracellular matrix components could determine additional functionality. The recruitment, targeting, and asymmetric distribution of activated Rac1/2 to plasma membrane components, could then cause the observed migration towards the necrotizing stimulus (Singh and Bhat, 2012; Laurila et al., 2009; Sakai et al., 2003; Zervas et al., 2001; Angers-Loustau et al., 1999; Tamura et al., 1998). Superoxide dismutase (*sod2* or *sod3*), may also contribute to the preparedness of the cell to move. Thus, a compromised cell–cell/ cell–matrix interaction coupled with an uninterrupted cell cycle constitutes an essential pre-requisite for most cells to initiate migration (Sukumaran et al., 2013; Connor et al., 2007; Ueno et al., 2006; Kubens et al., 2001). Evidence for a redistribution of ECSOD, both primary (R213G), and secondary to oxidative cleavage with subsequent dissociation with the ECM, results in a heightened inflammatory propensity, due to enhanced phagocyte migration (Kwon et al., 2015; Gottfredsen et al., 2014;

Yao et al., 2010; Gao et al., 2008).

3. The above discussion, also suggests, that the final concentration of RRA_{8+} may be the result of a complex signal transduction network, with H_2O_2 as the principal hub. There is a considerable volume of investigative work that highlights the role of this dismutated product of O_2^- as a modifier of the active transcriptome (Oshikawa et al., 2010; Vepa et al., 1999; DalleDonne et al., 1995). The preferred mechanism(s) of transduction, is the inhibition of phosphatase activity and subsequent hyper-phosphorylation, with the activation of mitogen-activated protein kinases (p38^{MAPK}, MEK, ERK2), and Axl-kinase activities (Huang et al., 2013; Andrew and Insall, 2007; Fischer et al., 2005; Usatyuk et al., 2003; Vepa et al., 1999; Hastie et al., 1998; Natarajan et al., 1996). Although, most of these enhance the migratory potential of the cell, the observation of the converse, *i.e.*, stasis, senescence and growth arrest; emphasizes the need to incorporate this additional complexity in any representative model. These roles of H_2O_2 are dependent on several modules operating in tandem. Whilst, module 1 could be transmembrane transport, module 2 could represent the effect of exigent modifiers such as growth factors, pharmacologic, and infective agents on secondary messengers; module 3, could constitute the regulatory effects of the plasma membrane components, ECM, and the cytoskeleton itself. An integrated model for dominant membrane folding using one or more of the simulated components is presented (Fig. 6).

3.3. A model for superoxide anion dependent lamellipodium formation

The residual fraction of cellular ROS ($\Delta \tau^0$) or the hydrogen peroxide formed by ECSOD after cell injury, could constitute a stimulus gradient to a circulating phagocyte. The transient and random membrane protrusions may function as sensors, and determine the proximity of the chemical moiety. Subsequent import or diffusion of ROS/ RNS into the cytoplasm of the responding cell may facilitate GTP-loading and activation of the small molecule Rac1/2 by *sod3*, prior to being secreted. The rapid membrane recruitment leads to a delocalized presence of GTPase-competent Rac1/2 and a generation of branched actin stress fibres throughout the cell. This transient cytoskeletal arrangement is modified by the fluctuating redox potential, as the cell ascertains, by repeated sampling, the optimal concentration of the inducing ROS. The assembly of lower order RRA-complexes (RRA, RRA_2, RRA_4) is short lived in the absence of consolidation, and constitutes a free radical futile cycle (Fig. 5B). As the membrane exposed local concentration of ROS increases, heightened import coupled with proton influx ($NADPH + 2O_2 \rightleftharpoons 2O_2^- + H^+ + NADP$), could constitute a localizing signal for focal recruitment and accumulation of high order RRA-complexes to specific zones on the membrane. Generalized phosphatase inactivation secondary to H_2O_2 accumulation could also complement this, by creating zones of high charge density (phosphorylation) of focal adhesion (p125, p68, vinculin) and integrin linked proteins. As the density of the Rac1/2 containing NAD(P)H-oxidase *viz.* RRA_{8+}, exceeds a critical concentration ($> 0.08aM$), the superoxide anions generated render any residual ECSOD ineffective (oxidative cleavage of HBD), whilst perturbing the membrane itself significantly for a longer time priod (Figs. 5B and 6). In a major cytoskeleton remodeling event, the now polarized RRA_{8+} could generate a secondary, focused, and sustained oxidative burst, thereby, reinitiating actin polymerization and culminating in a genesis of a single-formed directional specific lamellipodium (Fig. 6). Plasma membrane dynamics are characterized by gel–sol transitions, governed principally by the unsaturated fatty-acyl chains of the lipid bilayer (Wu et al., 2013; Ye et al., 2010; Brunauer et al., 1994). Stable remodeling, mandates

decreased fluidity, and is brought about by the peroxidation and consequent shortening of membrane lipids. These processes are likely to be linked to heightened, synchronous, and sustained generation of superoxide anions from the RRA_{8+} oligomers.

4. Methods

4.1. Computational tools

R-3.0.0, was downloaded and installed locally. The packages utilized with this distribution include GillespieSSA, an R implementation of the stochastic simulation algorithm. All codes (PERL- and R-scripts) were written in-house. The models constructed were static (SSM1-2) and dynamic (DSM1-4).

4.2. Mathematical models

4.2.1. Static stochastic models

The evolutionary dynamics of select plasma membrane regions on a phagocyte competent cell, hereby, referred to as nodes, were investigated using putative chemical inducers to influence membrane dynamics Eq. (11). In the absence of overt cellular injury, much of these would be scavenged thereby, minimizing the exposure to, and potentially limiting migration.

$$\left(a = \sqrt{\left(b_i - n_i \right)^2 + \left(b_j - n_j \right)^2 + \left(b_k - n_k \right)^2} \right) \tag{11}$$

a := distance metric($0 < a < 1; a \in \mathbb{R}$)

b := position of centroid of a hypothetical chemical inducer

n := centroid of anode

The proximity of the potential inducer(s), notwithstanding, the half-lives of these appear to be critical to dictating chemotaxis. Whilst, the SSM1 represented a possible physiological state (Dataset S1); SSM2, was formulated to demonstrate the plausibility of a molecular switch (Dataset S2). In these modifications of the Monte Carlo method, random numbers $(N_{ssm1}=53; N_{ssm2}=62)$ (Tables 1, S1, and S2) were selected from the open interval (0, 1), i.e., $0 < b < 1$.:

Table 2
Details of dynamic stochastic models.

R1	R2	P1	P2	Rn	DSM1	DSM2	DSM3	DSM4
Rac_GDP	GTP	Rac_GTP		1	$1.00*10^0$	$1.00*10^0$	$1.00*10^0$	$1.00*10^0$
	Rac_GTP	Rac_GDP		2	$1.00*10^2$	$1.00*10^2$	$1.00*10^2$	$1.00*10^2$
Rac_GTP	F-actin	RRA		3	$1.00*10^0$	$1.00*10^0$	$1.00*10^0$	$1.00*10^0$
	RRA	Rac_GTP	F-actin	4	$9.001*10^1$	$9.001*10^1$	$9.001*10^1$	$9.001*10^1$
NADPH	O_2	O_2^-		11	$1.00*10^0$	$1.00*10^0$	$1.00*10^0$	$1.00*10^0$
	O_2^-	NADPH	O_2	12	$1.00*10^6$	$1.00*10^6$	$1.00*10^6$	$1.00*10^6$
SOD	$2(O_2^-)$	H_2O_2		19	$1.00*10^0$	$1.00*10^0$	$1.00*10^0$	$1.00*10^0$
	H_2O_2	SOD	$2(O_2^-)$	20	$5.55*10^2$	$5.55*10^4$	$5.55*10^6$	$5.55*10^5$
	$2(RRA)$	$(RRA)_2$		5	$1.00*10^0$	$1.00*10^0$	$1.00*10^0$	$1.00*10^0$
	$(RRA)_2$	$2(RRA)$		6	$6.00*10^5$	$4.09*10^6$	$1.55*10^8$	$2.19*10^9$
2(NADPH)	$2(O_2^-)$	$2(O_2^-)$		13	$1.00*10^0$	$1.00*10^0$	$1.00*10^0$	$1.00*10^0$
	$2(O_2^-)$	2(NADPH)	$2(O_2)$	14	$1.00*10^6$	$1.00*10^6$	$1.00*10^6$	$1.00*10^6$
SOD	$2(O_2^-)$	H_2O_2		21	$1.00*10^0$	$1.00*10^0$	$1.00*10^0$	$1.00*10^0$
	H_2O_2	SOD	$2(O_2^-)$	22	$5.55*10^2$	$5.55*10^4$	$5.55*10^6$	$5.55*10^5$
	$2(RRA)_2$	$(RRA)_4$		7	$1.00*10^0$	$1.00*10^0$	$1.00*10^0$	$1.00*10^0$
	$(RRA)_4$	$2(RRA)_2$		8	$5.00*10^5$	$3.70*10^6$	$1.40*10^8$	$2.00*10^9$
4(NADPH)	$4(O_2)$	$4(O_2^-)$		15	$1.00*10^0$	$1.00*10^0$	$1.00*10^0$	$1.00*10^0$
	$4(O_2^-)$	4(NADPH)	$4(O_2)$	16	$1.00*10^6$	$1.00*10^6$	$1.00*10^6$	$1.00*10^6$
SOD	$2(O_2^-)$	H_2O_2		23	$1.00*10^0$	$1.00*10^0$	$1.00*10^0$	$1.00*10^0$
	H_2O_2	SOD	$2(O_2^-)$	24	$5.55*10^2$	$5.55*10^4$	$5.55*10^6$	$5.55*10^5$
	$2(RRA)_4$	$(RRA)_8$		9	$1.00*10^0$	$1.00*10^0$	$1.00*10^0$	$1.00*10^0$
	$(RRA)_8$	$2(RRA)_4$		10	$1.01*10^0$	$1.01*10^0$	$1.01*10^0$	$1.01*10^0$
8(NADPH)	$8(O_2)$	$8(O_2^-)$		17	$1.00*10^0$	$1.00*10^0$	$1.00*10^0$	$1.00*10^0$
	$8(O_2^-)$	8(NADPH)	$8(O_2)$	18	$1.00*10^6$	$1.00*10^6$	$1.00*10^6$	$1.00*10^6$
SOD	$2(O_2^-)$	H_2O_2		25	$1.00*10^0$	$1.00*10^0$	$1.00*10^0$	$1.00*10^0$
	H_2O_2	SOD	$2(O_2^-)$	26	$5.55*10^2$	$5.55*10^4$	$5.55*10^6$	$5.55*10^5$

Abbreviations
R1: Reactant 1
R2: Reactant 2
P1: Product 1
P2: Product 2
Rn: Reaction number
RRA: Rac-Raft-Actin
NADPH: Nicotinamide adenine dinucleotide phosphate
SOD: Superoxide dismutase
H_2O_2: Hydrogen peroxide
O_2: Molecular dioxygen
O_2^-: Superoxide anions
GDP: Guanosine diphosphate
GTP: Guanosine triphosphate
Mxx: Rate constants.

$$P_{ij}^{final} = max\left(P_{ij} \Big/ \sum_{j=1}^{j=6} P_{ij} \right) \qquad (12)$$

i = Number of observations$(i \in \{53, 62\})$

j = Nodes sampled for each observation$(j=6)$

k = $(i-1)^{th}$observation

P_{ij}^{final} = Final probability of i^{th}observation of j clusters of nodes

4.2.2. Dynamic stochastic models

A chemical master equation was formulated utilizing, as components, the lipid raft organization, NADP(H) oxidase, and actin oligomers (Tables 1 and 2). The rationale to choose arbitrary, *albeit*, linked rate constants was the speculative nature of the pathway itself, *i.e.*, stimulus-interstitium-cell. The solution to this equation was obtained numerically using an unmodified Gillespies's stochastic simulation algorithm (Gillespie et al., 2009; Gillespie, 2007). The preliminary data generated was with the simulation conditions as outlined (Table 2, S2; Datasets S3-S6). Here, an *in silico* experiment, entailed a simulation run/ observation of 600 s, $(N_i=30)$. This was conducted in triplicate, $(N_j=3)$. Miscellaneous parameters such as console interval, time units $(tf_i=100)$, etc., were in accordance with the package guidelines (GillespieSSA). Linear models (LM) relating the quantity of each metabolite $\left(y_{ij}^{k}\right)$ with the timestep associated with its computed values (μ_{ij}) were formulated. The coefficients computed were the estimate, standard error, t-value, and the probability of error $(pr > |t - value|)$, for the intercept (λ) and F-statistic of the observed values of the metabolite other than the test $\left(\theta_i^k\right)$, *i.e.*, $df=28;((30-1)-1)$ (Text S1–S4). The stochastic median of these timesteps $\left(\beta:=\text{median}\left(\bigcup_{i=1}^{i=90}\mu_{ij}\right)\right)$, was incorporated into the linear model appropriate for the metabolite $\left(LM_j^k\right)$, and used to intrapolate its quantity. The final values were mean and standard deviation values of these experiments $\left(\bar{LM}^k; \sigma\left(LM^k\right)\right)$ (Table S3).

$$LM_j^k = (\beta)\left(\theta_i^k\right) + \lambda_j^k \qquad (13)$$

4.2.3. Regression models

Scatter plots of the available ECSOD with the concentrations of the RRA complexes, collated from the DSMs were fitted to nonlinear regression curves (Fig. 3, Table S3). The choice of the regression equation was the coefficient of determination $(R^2=1)$ and/ or data variance (σ^2). The parameters examined were changes in the levels of generated superoxide anions and RRA-complexes. Whilst, the stoichiometry of the O_2^- generating NADPH complex $\left(RRA:O_2^- 1:1\right)$, dictated the number of superoxide anions, *i.e.*, $N_{O_2^-}(RRA)=1; N_{O_2^-}(RRA_2)=2; N_{O_2^-}(RRA_4)=4; N_{O_2^-}(RRA_8)=8$; their proportions were utilized to numerically compute a critical threshold, which could function as a molecular switch. A sequence of datapoints $(0 \le x \le 50000; 0 < x \le 1000; x:=ECSOD)$, in linear increments of 500 $(N_{obs}=101)$ and 1 $(N_{obs}=1000)$ was used with Eqs. (4, 6–9) (Tables S4B, S5B, S6) to establish trends in superoxide anion fluctuation.

4.3. Threshold definition

The molecular repertoire of the cell is extensive and redundant, with several examples of overlapping function. In comparison, cellular behavior is stochastic in the absence of any perturbation. A stimulus or an exigent event, with its incidental bias can polarize the underlying network of molecules into adopting a dominant state. The observable physiology could then be a threshold-dependent summation of all these. This quasi-binary switch is clearly dependent on a system defined limit (ω) (Table S4C), and differentiates the on–off state, *i.e.*, absence and unequivocal monotonic development of a dominant plasma membrane extension. In this work, I have used the individual concentrations of the mono- and oligo-mers of the RRA-complexes $\left(RRA_n, n \in \{1,2,4,8\}\right)$, or their ratios, thereof, in the DSMs to determine this, as under:

$$\omega = \log(\alpha), 0 < \omega <1, \alpha \in \left\{ \Psi_{12}, \Psi_{24}, \Psi_{48} \right\} \qquad (14)$$

Ψ_{12} := RRA_1/RRA_2
Ψ_{24} := RRA_2/RRA_4
Ψ_{48} := RRA_4/RRA_8

4.4. Establishing the zone of minimal fluctuation

The resultant data were descriptively summarized and analyzed. Non-decreasing sequences of slope values in the non-negative range of Eq. (13) (Table S7) were utilized to establish the steady-state zone of this curve $(15000 \le x \le 26000; y \cong 46000; N = 23)$. Here, the curve was divided into three regions such that $a_k \in (0,15000)$, $b_k \in [15000,26000]$, $c_k \in (26000,42825]$, and

S := $c_1, c_2, ... c_k$
$\quad : c_k = \left(|SO_{bmin} - SO_{bmax+k}|\right)/\left(|ECSOD_{bmin} - ECSOD_{bmax+k}|\right)$
T := $a_1, a_2, ... a_k: a_k = \left(|SO_{bmax} - SO_{bmin-(n-k+1)}|\right)$
$\qquad /\left(|ECSOD_{bmax} - ECSOD_{bmin-(n-k+1)}|\right)$

b_k := $\left(|SO_{bmin} - SO_{bmax}|\right)/\left(|ECSOD_{bmin} - ECSOD_{bmax}|\right)$
$\quad = \left(|SO_{bmax} - SO_{bmin}|\right)$
$\qquad /\left(|ECSOD_{bmax} - ECSOD_{bmin}|\right)$

$\because \Delta SO_b < \Delta SO_c, \Delta SO_b < \Delta SO_a;$
$\Delta ECSOD_b < \Delta ECSOD_c, \Delta ECSOD_b < \Delta ECSOD_a;$
$\Delta SO < \Delta ECSOD;$

It follows that:

$(\Delta SO_b + \delta_1/\Delta ECSOD_b + \delta_2) = (\Delta SO_c/\Delta ECSOD_c)$
$(\Delta SO_b + \delta_1/\Delta ECSOD_b + \delta_2) = (\Delta SO_a/\Delta ECSOD_a)$

Assume: $\delta_2 = \varepsilon_1 + \varepsilon_2; \delta_2 > \delta_1; \varepsilon_1 \gg \varepsilon_2$

$(\Delta SO_b/\Delta ECSOD_b) \le (\Delta SO_b + \delta_1/\Delta ECSOD_b + \varepsilon_1) < (\Delta SO_c/\Delta ECSOD_c)$ (i)

Similarly,

$(\Delta SO_b/\Delta ECSOD_b) \le (\Delta SO_b + \delta_1/\Delta ECSOD_b + \varepsilon_1) < (\Delta SO_a/\Delta ECSOD_a)$ (ii)

From (i) and (ii)

$$b_k < c_k; b_k < a_k \qquad (15,16)$$

5. Conclusion

The molecular and pathway redundancy of a cell renders its response to exigent stimuli 'fuzzy'. In this work, I have discussed the role of phagocyte chemotaxis in a microenvironment of graded

inflammatory signals, and the mechanisms of perceiving these, at the cellular level. Critical to these ideas is a distributed sensing mechanism with amplification, and an integrator(s). Whilst, the former could endow the responding cell a rapid reaction time, the latter would partition the response with the introduction of a 'lag'. This analysis also suggests that free radicals are justifiable candidates to streamline these processes, and that unlike other transduction mechanisms, these are sensitive to exogenous influence, self-limiting, and rapidly renewable. Further, the cell is able to utilize its myriad components to channelize, and, thereby, regulate its free radical pathways to fructify and modulate a complex cellular response. Pertubations have been shown to result in inefficient phagocytosis, increased susceptibility to infection, chronic inflammation, progress to malignancy, autoimmune diseases, inappropriate allergies, and hypersensitive reactions. Whilst, the mystery of stimulus directed movement is far from resolved, unraveling the underlying molecular processes that govern chemotaxis will advance our comprehension of several dependent phenomena in health and disease.

Author contribution

SK designed the study, formulated the models, conducted the simulations, collated and analyzed the data, wrote all the necessary code and the manuscript.

Conflict of interest

The author declares no competing financial interests.

Funding

The author received no specific funding for this work.

Appendix A. Supplementary material

Supplementary data associated with this article can be found in the online version at http://dx.doi.org/10.1016/j.jtbi.2016.07.002.

References

Allen, W.E., Jones, G.E., Pollard, J.W., Ridley, A.J., 1997. Rho, Rac and Cdc42 regulate actin organization and cell adhesion in macrophages. J. Cell Sci. 110 (Pt 6), 707–720.

Andrew, N., Insall, R.H., 2007. Chemotaxis in shallow gradients is mediated independently of PtdIns 3-kinase by biased choices between random protrusions. Nat. Cell Biol. 9, 193–200.

Angers-Loustau, A., Cote, J.F., Tremblay, M.L., 1999. Roles of protein tyrosine phosphatases in cell migration and adhesion. Biochem. Cell Biol.=Biochim. Biol. Cell. 77, 493–505.

Babior, B.M., 1999. NADPH oxidase: an update. Blood 93, 1464–1476.

Banan, A., Zhang, Y., Losurdo, J., Keshavarzian, A., 2000. Carbonylation and disassembly of the F-actin cytoskeleton in oxidant induced barrier dysfunction and its prevention by epidermal growth factor and transforming growth factor alpha in a human colonic cell line. Gut 46, 830–837.

Bianchini, L., Todderud, G., Grinstein, S., 1993. Cytosolic [Ca2+] homeostasis and tyrosine phosphorylation of phospholipase C gamma 2 in HL60 granulocytes. J. Biol. Chem. 268, 3357–3363.

Borkovich, K.A., Kaplan, N., Hess, J.F., Simon, M.I., 1989. Transmembrane signal transduction in bacterial chemotaxis involves ligand-dependent activation of phosphate group transfer. Proc. Natl. Acad. Sci. USA 86, 1208–1212.

Brown, P.N., Hill, C.P., Blair, D.F., 2002. Crystal structure of the middle and C-terminal domains of the flagellar rotor protein FliG. EMBO J. 21, 3225–3234.

Brunauer, L.S., Moxness, M.S., Huestis, W.H., 1994. Hydrogen peroxide oxidation induces the transfer of phospholipids from the membrane into the cytosol of human erythrocytes. Biochemistry 33, 4527–4532.

Cammarota, F., de Vita, G., Salvatore, M., Laukkanen, M.O., 2015. Ras oncogene-mediated progressive silencing of extracellular superoxide dismutase in tumorigenesis. Biomed. Res. Int. 2015, 780409.

Castellone, M.D., Langella, A., Cantara, S., Laurila, J.P., Laatikainen, L.E., Bellelli, R., Pacini, F., Salvatore, M., Laukkanen, M.O., 2014. Extracellular superoxide dismutase induces mouse embryonic fibroblast proliferative burst, growth arrest, immortalization, and consequent in vivo tumorigenesis. Antioxid.Redox Signal. 21, 1460–1474.

Chen, H.C., Guan, J.L., 1994. Stimulation of phosphatidylinositol 3′-kinase association with foca adhesion kinase by platelet-derived growth factor. J. Biol. Chem. 269, 31229–31233.

Connor, K.M., Hempel, N., Nelson, K.K., Dabiri, G., Gamarra, A., Belarmino, J., Van De Water, L., Mian, B.M., Melendez, J.A., 2007. Manganese superoxide dismutase enhances the invasive and migratory activity of tumor cells. Cancer Res. 67, 10260–10267.

DalleDonne, I., Milzani, A., Colombo, R., 1995. H2O2-treated actin: assembly and polymer interactions with cross-linking proteins. Biophys. J. 69, 2710–2719.

Danielson, M.A., Biemann, H.P., Koshland Jr., D.E., Falke, J.J., 1994. Attractant- and disulfide-induced conformational changes in the ligand binding domain of the chemotaxis aspartate receptor: a 19F NMR study. Biochemistry 33, 6100–6109.

Decleva, E., Menegazzi, R., Fasolo, A., Defendi, F., Sebastianutto, M., Dri, P., 2013. Intracellular shunting of O2, contributes to charge compensation and preservation of neutrophil respiratory burst in the absence of voltage-gated proton channel activity. Exp. Cell Res. 319, 1875–1888.

Derevianko, A., D'Amico, R., Graeber, T., Keeping, H., Simms, H.H., 1997. Endogenous PMN-derived reactive oxygen intermediates provide feedback regulation on respiratory burst signal transduction. J. Leukoc. Biol. 62, 268–276.

del Pozo, M.A., Alderson, N.B., Kiosses, W.B., Chiang, H.H., Anderson, R.G., Schwartz, M.A., 2004. Integrins regulate Rac targeting by internalization of membrane domains. Science 303, 839–842.

Edgington, M.P., Tindall, M.J., 2015. Understanding the link between single cell and population scale responses of Escherichia coli in differing ligand gradients. Comput. Struct. Biotechnol. J. 13, 528–538.

Fischer, S., Wiesnet, M., Renz, D., Schaper, W., 2005. H2O2 induces paracellular permeability of porcine brain-derived microvascular endothelial cells by activation of the p44/42 MAP kinase pathway. Eur. J. cell Biol. 84, 687–697.

Fisher, A.B., 2009. Redox signaling across cell membranes. Antioxid. Redox Signal. 11, 1349–1356.

Folz, R.J., Peno-Green, L., Crapo, J.D., 1994. Identification of a homozygous missense mutation, Arg to Gly in the critical binding region of the human EC-SOD gene, SOD3 and its association with dramatically increased serum enzyme levels. Human. Mol. Genet. 3, 2251–2254.

Forman, H.J., Fukuto, J.M., Torres, M., 2004. Redox signaling: thiol chemistry defines which reactive oxygen and nitrogen species can act as second messengers. Am. J. Physiol. Cell Physiol. 287, C246–256.

Fukata, M., Nakagawa, M., Kaibuchi, K., 2003. Roles of Rho-family GTPases in cell polarisation and directional migration. Curr. Opin. Cell Biol. 15, 590–597.

Gao, F., Koenitzer, J.R., Tobolewski, J.M., Jiang, D., Liang, J., Noble, P.W., Oury, T.D., 2008. Extracellular superoxide dismutase inhibits inflammation by preventing oxidative fragmentation of hyaluronan. J. Biol. Chem. 283, 6058–6066.

Gillespie, D.T., 2007. Stochastic simulation of chemical kinetics. Annu. Rev. Phys. Chem. 58, 35–55.

Gillespie, D.T., Roh, M., Petzold, L.R., 2009. Refining the weighted stochastic simulation algorithm. J. Chem. Phys. 130, 174103.

Giustarini, D., Milzani, A., Aldini, G., Carini, M., Rossi, R., Dalle-Donne, I., 2005. S-nitrosation versus S-glutathionylation of protein sulfhydryl groups by S-nitrosoglutathione. Antioxid. Redox Signal. 7, 930–939.

Gottfredsen, R.H., Goldstrohm, D.A., Hartney, J.M., Larsen, U.G., Bowler, R.P., Petersen, S.V., 2014. The cellular distribution of extracellular superoxide dismutase in macrophages is altered by cellular activation but unaffected by the naturally occurring R213G substitution. Free Radic. Biol. Med. 69, 348–356.

Grigoriev, I., Borisy, G., Vorobjev, I., 2006. Regulation of microtubule dynamics in 3T3 fibroblasts by Rho family GTPases. Cell Motil. Cytoskelet. 63, 29–40.

Guidobaldi, H.A., Teves, M.E., Unates, D.R., Anastasia, A., Giojalas, L.C., 2008. Progesterone from the cumulus cells is the sperm chemoattractant secreted by the rabbit oocyte cumulus complex. PloS One 3, e3040.

Guyton, K.Z., Liu, Y., Gorospe, M., Xu, Q., Holbrook, N.J., 1996. Activation of mitogen-activated protein kinase by H2O2. Role in cell survival following oxidant injury. J. Biol. Chem. 271, 4138–4142.

Hastie, L.E., Patton, W.F., Hechtman, H.B., Shepro, D., 1998. Metabolites of the phospholipase D pathway regulate H2O2-induced filamin redistribution in endothelial cells. J. Cell. Biochem. 68, 511–524.

Hattori, H., Subramanian, K.K., Sakai, J., Luo, H.R., 2010. Reactive oxygen species as signaling molecules in neutrophil chemotaxis. Commun. Integr. Biol. 3, 278–281.

Hawkins, B.J., Madesh, M., Kirkpatrick, C.J., Fisher, A.B., 2007. Superoxide flux in endothelial cells via the chloride channel-3 mediates intracellular signaling. Mol. Biol. Cell 18, 2002–2012.

Huang, J.S., Cho, C.Y., Hong, C.C., Yan, M.D., Hsieh, M.C., Lay, J.D., Lai, G.M., Cheng, A.L., Chuang, S.E., 2013. Oxidative stress enhances Axl-mediated cell migration through an Akt1/Rac1-dependent mechanism. Free Radic. Biol. Med. 65, 1246–1256.

Jin, H., Yu, Y., Hu, Y., Lu, C., Li, J., Gu, J., Zhang, L., Huang, H., Zhang, D., Wu, X.R., et al., 2015. Divergent behaviors and underlying mechanisms of cell migration and invasion in non-metastatic T24 and its metastatic derivative T24T bladder cancer cell lines. Oncotarget 6, 522–536.

Karlsson, K., Sandstrom, J., Edlund, A., Marklund, S.L., 1994. Turnover of extra-cellular-superoxide dismutase in tissues. Lab. Investig. J. Tech. Methods Pathol. 70, 705–710.

Kawakami, N., Shimohama, S., Hayakawa, T., Sumida, Y., Fujimoto, S., 1996. Tyrosine phosphorylation and translocation of phospholipase C-gamma 2 in poly-morphonuclear leukocytes treated with pervanadate. Biochim. Biophys. acta 1314, 167–174.

Kim, S.H., Kim, K.H., Yoo, B.C., Ku, J.L., 2012. Induction of LGR5 by H2O2 treatment is associated with cell proliferation via the JNK signaling pathway in colon cancer cells. Int. J. Oncol. 41, 1744–1750.

Kubens, B.S., Niggemann, B., Zanker, K.S., 2001. Prevention of entrance into G2 cell cycle phase by mimosine decreases locomotion of cells from the tumor cell line SW480. Cancer Lett. 162, S39–S47.

Kundu, S., 2015a. Co-operative intermolecular kinetics of 2-oxoglutarate dependent dioxygenases may be essential for system-level regulation of plant cell phy-siology. Front. Plant Sci. 6, 489.

Kundu, S., 2015b. Unity in diversity, a systems approach to regulating plant cell physiology by 2-oxoglutarate-dependent dioxygenases. Front. Plant Sci. 6, 98.

Kundu, S., Subodh, S., 2011. Gradient sensing in vectorial chemotaxis – a novel role for reactive oxygen species. Int. J. trends Med. 1, 54–59.

Kwon, M.J., Lee, K.Y., Lee, H.W., Kim, J.H., Kim, T.Y., 2015. SOD3 Variant, R213G, Altered SOD3 Function, Leading to ROS-Mediated Inflammation and Damage in Multiple Organs of Premature Aging Mice. Antioxid. Redox Signal. 23, 985–999.

Laukkanen, M.O., Cammarota, F., Esposito, T., Salvatore, M., Castellone, M.D., 2015. Extracellular superoxide dismutase regulates the expression of small gtpase regulatory proteins GEFs, GAPs, and GDI. PloS One 10, e0121441.

Laurila, J.P., Laatikainen, L.E., Castellone, M.D., Laukkanen, M.O., 2009. SOD3 reduces inflammatory cell migration by regulating adhesion molecule and cytokine expression. PloS One 4, e5786.

Lin, W.C., Wang, L.C., Pang, T.L., Chen, M.Y., 2015. Actin-binding protein G, AbpG participates in modulating the actin cytoskeleton and cell migration in Dic-tyostelium discoideum. Mol. Biol. Cell 26, 1084–1097.

Liu, Z., He, Q., Ding, X., Zhao, T., Zhao, L., Wang, A., 2015. SOD2 is a C-myc target gene that promotes the migration and invasion of tongue squamous cell car-cinoma involving cancer stem-like cells. Int. J. Biochem. Cell Biol. 60, 139–146.

Liu, H., Zhang, H., Forman, H.J., 2007. Silica induces macrophage cytokines through phosphatidylcholine-specific phospholipase C with hydrogen peroxide. Am. J. Respir. Cell Mol. Biol. 36, 594–599.

Luo, B.H., Carman, C.V., Springer, T.A., 2007. Structural basis of integrin regulation and signaling. Annu. Rev. Immunol. 25, 619–647.

Marklund, S.L., 1982. Human copper-containing superoxide dismutase of high molecular weight. Proc. Natl. Acad. Sci. USA 79, 7634–7638.

Miar, A., Hevia, D., Munoz-Cimadevilla, H., Astudillo, A., Velasco, J., Sainz, R.M., Mayo, J.C., 2015. Manganese superoxide dismutase, SOD2/MnSOD/catalase and SOD2/GPx1 ratios as biomarkers for tumor progression and metastasis in prostate, colon, and lung cancer. Free Radic. Biol. Med. 85, 45–55.

Mikkelsen, R.B., Wardman, P., 2003. Biological chemistry of reactive oxygen and nitrogen and radiation-induced signal transduction mechanisms. Oncogene 22, 5734–5754.

Moldovan, L., Irani, K., Moldovan, N.I., Finkel, T., Goldschmidt-Clermont, P.J., 1999. The actin cytoskeleton reorganization induced by Rac1 requires the production of superoxide. Antioxid. Redox Signal. 1, 29–43.

Nagy, K., Sipos, O., Valkai, S., Gombai, E., Hodula, O., Kerenyi, A., Ormos, P., Galajda, P., 2015. Microfluidic study of the chemotactic response of Escherichia coli to amino acids, signaling molecules and secondary metabolites. Biomicrofluidics 9, 044105.

Natarajan, V., Vepa, S., Verma, R.S., Scribner, W.M., 1996. Role of protein tyrosine phosphorylation in H2O2-induced activation of endothelial cell phospholipase D. Am. J. Physiol. 271, L400–408.

NicolauJr, D.V., Burrage, K., Parton, R.G., Hancock, J.F., 2006. Identifying optimal li-pid raft characteristics required to promote nanoscale protein-protein inter-actions on the plasma membrane. Mol. Cell Biol. 26 (1), 313–323, PubMed PMID: 16354701; PubMed Central PMCID: PMC1317633.

Nimnual, A.S., Taylor, L.J., Bar-Sagi, D., 2003. Redox-dependent downregulation of Rho by Rac. Nat. Cell Biol. 5, 236–241.

Nobes, C.D., Hall, A., 1995. Rho, rac, and cdc42 GTPases regulate the assembly of multimolecular focal complexes associated with actin stress fibers, lamellipo-dia, and filopodia. Cell 81, 53–62.

Olsen, D.A., Petersen, S.V., Oury, T.D., Valnickova, Z., Thogersen, I.B., Kristensen, T., Bowler, R.P., Crapo, J.D., Enghild, J.J., 2004. The intracellular proteolytic pro-cessing of extracellular superoxide dismutase, EC-SOD is a two-step event. J. Biol. Chem. 279, 22152–22157.

Oshikawa, J., Urao, N., Kim, H.W., Kaplan, N., Razvi, M., McKinney, R., Poole, L.B., Fukai, T., Ushio-Fukai, M., 2010. Extracellular SOD-derived H2O2 promotes VEGF signaling in caveolae/lipid rafts and post-ischemic angiogenesis in mice. PloS One 5, e10189.

Park, I.J., Hwang, J.T., Kim, Y.M., Ha, J., Park, O.J., 2006. Differential modulation of AMPK signaling pathways by low or high levels of exogenous reactive oxygen species in colon cancer cells. Ann. N. Y. Acad. Sci. 1091, 102–109.

Pasupuleti, S., Sule, N., Cohn, W.B., MacKenzie, D.S., Jayaraman, A., Manson, M.D., 2014. Chemotaxis of Escherichia coli to norepinephrine, NE requires conversion of NE to 3,4-dihydroxymandelic acid. J. Bacteriol. 196, 3992–4000.

Rocklin, A.M., Kato, K., Liu, H.W., Que Jr., L., Lipscomb, J.D., 2004. Mechanistic studies of 1-aminocyclopropane-1-carboxylic acid oxidase: single turnover reaction. J. Biol. Inorg. Chem.: JBIC: Publ. Soc. Biol. Inorg. Chem. 9, 171–182.

Sadhu, C., Masinovsky, B., Dick, K., Sowell, C.G., Staunton, D.E., 2003. Essential role

of phosphoinositide 3-kinase delta in neutrophil directional movement. J. Im-munol. 170, 2647–2654.

Sakai, T., Li, S., Docheva, D., Grashoff, C., Sakai, K., Kostka, G., Braun, A., Pfeifer, A., Yurchenco, P.D., Fassler, R., 2003. Integrin-linked kinase, ILK is required for polarizing the epiblast, cell adhesion, and controlling actin accumulation. Genes Dev. 17, 926–940.

Sastry, S.K., Lyons, P.D., Schaller, M.D., Burridge, K., 2002. PTP-PEST controls motility through regulation of Rac1. J. cell Sci. 115, 4305–4316.

Segota, I., Mong, S., Neidich, E., Rachakonda, A., Lussenhop, C.J., Franck, C., 2013. High fidelity information processing in folic acid chemotaxis of Dictyostelium amoebae. J. R. Soc. Interface/R. Soc. 10, 20130606.

Shi, D., Li, X., Chen, H., Che, N., Zhou, S., Lu, Z., Shi, S., Sun, L., 2014. High level of reactive oxygen species impaired mesenchymal stem cell migration via over-polymerization of F-actin cytoskeleton in systemic lupus erythematosus. Pa-thol. Biol. 62, 382–390.

Shimaoka, T., Nakayama, T., Hieshima, K., Kume, N., Fukumoto, N., Minami, M., Hayashida, K., Kita, T., Yoshie, O., Yonehara, S., 2004. Chemokines generally exhibit scavenger receptor activity through their receptor-binding domain. J. Biol. Chem. 279, 26807–26810.

Singh, B., Bhat, H.K., 2012. Superoxide dismutase 3 is induced by antioxidants, in-hibits oxidative DNA damage and is associated with inhibition of estrogen-in-duced breast cancer. Carcinogenesis 33, 2601–2610.

Srinivasan, K., Wright, G.A., Hames, N., Housman, M., Roberts, A., Aufderheide, K.J., Janetopoulos, C., 2013. Delineating the core regulatory elements crucial for directed cell migration by examining folic-acid-mediated responses. J. cell Sci. 126, 221–233.

Stralin, P., Marklund, S.L., 1994. Effects of oxidative stress on expression of extra-cellular superoxide dismutase, CuZn-superoxide dismutase and Mn-superoxide dismutase in human dermal fibroblasts. Biochem. J. 298 (Pt 2) 347–352.

Sukumaran, P., Lof, C., Pulli, I., Kemppainen, K., Viitanen, T., Tornquist, K., 2013. Significance of the transient receptor potential canonical 2, TRPC2 channel in the regulation of rat thyroid FRTL-5 cell proliferation, migration, adhesion and invasion. Mol. Cell. Endocrinol. 374, 10–21.

Tai, Y.T., Podar, K., Catley, L., Tseng, Y.H., Akiyama, M., Shringarpure, R., Burger, R., Hideshima, T., Chauhan, D., Mitsiades, N., et al., 2003. Insulin-like growth fac-tor-1 induces adhesion and migration in human multiple myeloma cells via activation of beta1-integrin and phosphatidylinositol 3′-kinase/AKT signaling. Cancer Res. 63, 5850–5858.

Tamura, M., Gu, J., Matsumoto, K., Aota, S., Parsons, R., Yamada, K.M., 1998. In-hibition of cell migration, spreading, and focal adhesions by tumor suppressor PTEN. Science 280, 1614–1617.

Torres, M., Forman, H.J., 2003. Redox signaling and the MAP kinase pathways. BioFactors 17, 287–296.

Tyson, R.A., Zatulovskiy, E., Kay, R.R., Bretschneider, T., 2014. How blebs and pseudopods cooperate during chemotaxis. Proc. Natl. Acad. Sci. USA 111, 11703–11708.

Tzima, E., 2006. Role of small GTPases in endothelial cytoskeletal dynamics and the shear stress response. Circ. Res. 98, 176–185.

Ueno, M., Katayama, K., Yamauchi, H., Nakayama, H., Doi, K., 2006. Cell cycle pro-gression is required for nuclear migration of neural progenitor cells. Brain Res. 1088, 57–67.

Usatyuk, P.V., Vepa, S., Watkins, T., He, D., Parinandi, N.L., Natarajan, V., 2003. Redox regulation of reactive oxygen species-induced p38 MAP kinase activation and barrier dysfunction in lung microvascular endothelial cells. Antioxid. Redox Signal. 5, 723–730.

Ushio-Fukai, M., 2009. Compartmentalization of redox signaling through NADPH oxidase-derived ROS. Antioxid. Redox Signal. 11, 1289–1299.

Van Keymeulen, A., Wong, K., Knight, Z.A., Govaerts, C., Hahn, K.M., Shokat, K.M., Bourne, H.R., 2006. To stabilize neutrophil polarity, PIP3 and Cdc42 augment RhoA activity at the back as well as signals at the front. J. Cell Biol. 174, 437–445.

Vepa, S., Scribner, W.M., Parinandi, N.L., English, D., Garcia, J.G., Natarajan, V., 1999. Hydrogen peroxide stimulates tyrosine phosphorylation of focal adhesion ki-nase in vascular endothelial cells. Am. J. Physiol. 277, L150–158.

Volberg, T., Geiger, B., Dror, R., Zick, Y., 1991. Modulation of intercellular adherens-type junctions and tyrosine phosphorylation of their components in RSV-transformed cultured chick lens cells. Cell Regul. 2, 105–120.

Watanabe, T., Wang, S., Noritake, J., Sato, K., Fukata, M., Takefuji, M., Nakagawa, M., Izumi, N., Akiyama, T., Kaibuchi, K., 2004. Interaction with IQGAP1 links APC to Rac1, Cdc42, and actin filaments during cell polarization and migration. Dev. cell 7, 871–883.

Weed, S.A., Karginov, A.V., Schafer, D.A., Weaver, A.M., Kinley, A.W., Cooper, J.A., Parsons, J.T., 2000. Cortactin localization to sites of actin assembly in lamelli-podia requires interactions with F-actin and the Arp2/3 complex. J. Cell Biol. 151, 29–40.

Weed, S.A., Parsons, J.T., 2001. Cortactin: coupling membrane dynamics to cortical actin assembly. Oncogene 20, 6418–6434.

Wessels, D., Lusche, D.F., Scherer, A., Kuhl, S., Myre, M.A., Soll, D.R., 2014. Huntingtin regulates Ca²⁺ chemotaxis and K⁺-facilitated cAMP chemotaxis, in conjunc-tion with the monovalent cation/H⁺ exchanger Nhe1, in a model develop-mental system: insights into its possible role in Huntingtons disease. Dev. Biol. 394, 24–38.

Wong, K., Pertz, O., Hahn, K., Bourne, H., 2006. Neutrophil polarization: spatio-temporal dynamics of RhoA activity support a self-organizing mechanism. Proc. Natl. Acad. Sci. USA 103, 3639–3644.

Wu, Q., Qi, B., Liu, Y., Cheng, B., Liu, L., Li, Y., Wang, Q., 2013. Mechanisms underlying protective effects of trimetazidine on endothelial progenitor cells biological

functions against H2O2-induced injury: involvement of antioxidation and Akt/eNOS signaling pathways. Eur. J. Pharmacol. 707, 87–94.

Wylie, D.C., Das, J., Chakraborty, A.K., 2007. Sensitivity of T cells to antigen and antagonism emerges from differential regulation of the same molecular signaling module. Proc. Natl. Acad. Sci. U S A 104 (13), 5533–5538, Epub 2007 Mar 2. PubMed PMID: 17360359; PubMed Central PMCID: PMC1838481.

Yao, H., Arunachalam, G., Hwang, J.W., Chung, S., Sundar, I.K., Kinnula, V.L., Crapo, J.D., Rahman, I., 2010. Extracellular superoxide dismutase protects against pulmonary emphysema by attenuating oxidative fragmentation of ECM. Proc. Natl. Acad. Sci. USA 107, 15571–15576.

Ye, S., Tan, L., Ma, J., Shi, Q., Li, J., 2010. Polyunsaturated docosahexaenoic acid suppresses oxidative stress induced endothelial cell calcium influx by altering lipid composition in membrane caveolar rafts. Prostaglandins Leukot. Essent. Fat. Acids 83, 37–43.

Yousif, A.M., Minopoli, M., Bifulco, K., Ingangi, V., Di Carluccio, G., Merlino, F., Motti, M.L., Grieco, P., Carriero, M.V., 2015. Cyclization of the urokinase receptor-derived ser-arg-ser-arg-tyr Peptide generates a potent inhibitor of trans-endothelial migration of monocytes. PloS One 10, e0126172.

Zervas, C.G., Gregory, S.L., Brown, N.H., 2001. Drosophila integrin-linked kinase is required at sites of integrin adhesion to link the cytoskeleton to the plasma membrane. J. Cell Biol. 152, 1007–1018.

Zhang, D., Wang, Y., Liang, Y., Zhang, M., Wei, J., Zheng, X., Li, F., Meng, Y., Zhu, N.W., Li, J., et al., 2014. Loss of p27 upregulates MnSOD in a STAT3-dependent manner, disrupts intracellular redox activity and enhances cell migration. J. Cell Sci. 127, 2920–2933.

Zhou, X., Li, D., Resnick, M.B., Behar, J., Wands, J., Cao, W., 2011. Signaling in H_2O_2-induced increase in cell proliferation in Barrett's esophageal adenocarcinoma cells. J. Pharmacol. Exp. Ther. 339, 218–227.